

Spectral statistics of interpolating random circulant matrix

Sunidhi Sen, Himanshu Shekhar, Santosh Kumar*

Department of Physics, Shiv Nadar Institution of Eminence (SNIoE), Gautam Buddha Nagar, Uttar Pradesh – 201314, India

E-mail:

sensunidhi96@gmail.com, himanshuphy02@gmail.com, *skumar.physics@gmail.com

Abstract. We consider a versatile matrix model of the form $\mathbf{A} + i\mathbf{B}$, where \mathbf{A} and \mathbf{B} are real random circulant matrices with independent but, in general, non-identically distributed Gaussian entries. For this model, we derive exact result for the joint probability density function and find that it is a multivariate Gaussian. Consequently, exact expression for arbitrary order marginal density also ensues. It is demonstrated that by adjusting the averages and variances of the Gaussian elements of \mathbf{A} and \mathbf{B} , we can interpolate between a remarkably wide range of eigenvalue distributions in the complex plane. In particular, we can examine the crossover between a random real circulant matrix and a random complex circulant matrix. We also extend our study to include Wigner-like and Wishart-like matrices constructed from our general random circulant matrix. To validate our analytical findings, Monte Carlo simulations are conducted, which confirm the accuracy of our results.

1 Introduction

Circulant matrices, a special type of Toeplitz matrices, exhibit a distinct pattern in which each row is formed by cyclically shifting the entries of the preceding row. This inherent symmetry and algebraic structure make circulant matrices immensely valuable across various domains of mathematics, physics, engineering, and computer science [1, 2]. They offer efficient solutions for a wide range of problems including difference and differential equations [3–7], graph theory [8, 9], time-series analysis [10–12], signal and image processing [13–16], computer vision [17, 18], cryptography [19], coding theory [20], vibrational analysis [21], statistical physics [22], quantum mechanics [23, 24], and more.

Random variants of circulant matrices have also received attention due to their natural occurrence in problems related to random walk [24], stochastic time series [10], 5G communication schemes [16], etc. Moreover, there is a natural curiosity regarding the behavior of their spectrum compared to the classical random matrices such as Wigner and Wishart [25, 26], as well as non-Hermitian Ginibre matrices [27, 28]. Notably, in references [29–31] the local spectral fluctuations of random circulant matrices have been studied using nearest neighbor distribution. Additionally, several interesting results,

including those pertaining to limiting spectral density and associated moments, can be found in references [32–34]. However, despite these significant contributions, there is still much to be explored, particularly in terms of exact results. The present work is an attempt to contribute in this direction.

We consider a very general N -dimensional complex circulant random matrix, $\mathbf{H} = \mathbf{A} + i\mathbf{B}$, where \mathbf{A} and \mathbf{B} are real-circulant matrices, whose entries have been chosen as Gaussian variates which are independent but in general taken from non-identical distributions. For this random matrix model, we derive an exact closed-form expression for the joint probability density function (JPDF) of all eigenvalues, revealing that it follows a multivariate Gaussian distribution. Consequently, we can readily obtain the exact marginal densities for any subset of eigenvalues. We show that the eigenvalues can exhibit a vast range of behavior in the complex plane as one tunes averages and variances of the Gaussian elements of \mathbf{A} and \mathbf{B} . In particular, the interpolation between real circulant and complex circulant random matrix can be realized. Finally, we also examine the eigenvalues of Wigner-like and Wishart-like matrices constructed out of \mathbf{H} . We also carry out Monte Carlo simulations and find the results thereof to be consistent with our analytical results.

The remaining of the paper is organised as follows. In section 2, we introduce our random circulant matrix model and derive the JPDF of real and imaginary parts of all eigenvalues. The expressions of various marginal densities are also provided in this section. Next, in section 3, we obtain explicit evaluations of covariance matrix and mean vector describing the JPDF derived in the preceding section, in terms of the variances and averages of the Gaussian elements of the matrices \mathbf{A} and \mathbf{B} . Some cases of special interest are also discussed in this section. Afterwards, in sections 4 and 5, we study Wigner-like and Wishart-like matrices constructed out of the random circulant matrix \mathbf{H} . Section 6 is dedicated to comparison of the results derived with Monte Carlo simulations. We conclude with a summary of our results along with discussion of some possible future directions in section 7.

2 A general random circulant matrix model

We consider the N -dimensional random circulant matrix, $\mathbf{H} = \mathbf{A} + i\mathbf{B}$, where \mathbf{A} and \mathbf{B} are two real circulant matrices having the forms:

$$\mathbf{A} = \begin{bmatrix} a_1 & a_N & \dots & a_2 \\ a_2 & a_1 & \dots & a_3 \\ \vdots & \vdots & \ddots & \vdots \\ a_N & a_{N-1} & \dots & a_1 \end{bmatrix}, \quad \mathbf{B} = \begin{bmatrix} b_1 & b_N & \dots & b_2 \\ b_2 & b_1 & \dots & b_3 \\ \vdots & \vdots & \ddots & \vdots \\ b_N & b_{N-1} & \dots & b_1 \end{bmatrix}. \quad (1)$$

The elements a_j and b_j , ($j = 1, \dots, N$), are taken to be independent but non-identical Gaussians, with corresponding averages and variances as u_j, v_j and σ_j^2, τ_j^2 , respectively.

Therefore, they are distributed as

$$P_a(\{a\}) = \prod_{j=1}^N \frac{1}{(2\pi\sigma_j^2)^{1/2}} \exp\left(-\frac{(a_j - u_j)^2}{2\sigma_j^2}\right), \quad (2)$$

$$P_b(\{b\}) = \prod_{j=1}^N \frac{1}{(2\pi\tau_j^2)^{1/2}} \exp\left(-\frac{(b_j - v_j)^2}{2\tau_j^2}\right). \quad (3)$$

The \mathbf{H} matrix therefore possesses the structure,

$$\mathbf{H} = \begin{bmatrix} h_1 & h_N & \dots & h_2 \\ h_2 & h_1 & \dots & h_3 \\ \vdots & \vdots & \ddots & \vdots \\ h_N & h_{N-1} & \dots & h_1 \end{bmatrix}, \quad (4)$$

with $h_r = (a_r + ib_r)$; $r = 1, \dots, N$. We note that the matrix model $\mathbf{H} = \alpha\mathbf{A} + \beta\mathbf{B}$, where α, β are real, can be mapped to the above model since α and β can be absorbed within the averages u_j, v_j and variances σ_j^2, τ_j^2 , yielding the modified averages and variances as $\alpha u_j, \beta v_j$ and $\alpha^2 \sigma_j^2, \beta^2 \tau_j^2$, respectively. We further observe that in the limit $v_j, \tau_j \rightarrow 0$ for $j = 1, \dots, N$, effectively only \mathbf{A} survives, i.e., \mathbf{H} is purely real. Similarly when $u_j, \sigma_j \rightarrow 0$ for $j = 1, \dots, N$, only \mathbf{B} survives so that \mathbf{H} is purely imaginary.

We are interested in the distribution of eigenvalues of \mathbf{H} and their dynamics in the complex plane as the averages and variances of the matrix elements of \mathbf{A} and \mathbf{B} are varied. From the properties of circulant matrix, we know that the eigenvalues of \mathbf{H} can be written as [1, 2],

$$\lambda_j = \sum_{r=1}^N h_r \omega_j^{(N-r+1)}; \quad j = 1, \dots, N, \quad (5)$$

where ω_j are the N th roots of unity,

$$\omega_j = \exp[i2\pi(j-1)/N]. \quad (6)$$

Moreover, the diagonalizing matrix \mathbf{U} for any circulant matrix is unitary and has matrix elements given by

$$U_{j,k} = \frac{1}{\sqrt{N}} \omega_j^{k-1}; \quad \dots, j, k = 1, \dots, N. \quad (7)$$

Expressing λ_j above in terms of the matrix elements of \mathbf{A} and \mathbf{B} , and separating the real and imaginary parts, we obtain

$$\begin{aligned} \lambda_j &= \sum_{r=1}^N (a_r C_{jr} - b_r S_{jr}) + i \sum_{r=1}^N (a_r S_{jr} + b_r C_{jr}) \\ &\equiv \eta_{2j-1} + i\eta_{2j}, \end{aligned} \quad (8)$$

where

$$C_{j,r} = \cos \left[\frac{2\pi(j-1)(N-r+1)}{N} \right], \quad (9)$$

$$S_{j,r} = \sin \left[\frac{2\pi(j-1)(N-r+1)}{N} \right]. \quad (10)$$

Therefore, the odd-indexed and even-indexed η 's are the real and imaginary parts of λ_j 's, respectively. These can be contained in a vector $\boldsymbol{\eta} = (\eta_1, \eta_2, \dots, \eta_{2N-1}, \eta_{2N})^T$, where T represents the transpose.

To obtain the joint distribution of λ 's, or equivalently that of η 's, we need to integrate over the Gaussian variables a_j and b_j . For compactness, let us define the following quantities. We consider a $2N$ -dimensional column vector \mathbf{h} comprising a_j and b_j as $\mathbf{h} = (a_1, b_1, \dots, a_N, b_N)^T$. Clearly, \mathbf{h} is governed by the multivariate Gaussian probability density function,

$$P_{\mathbf{h}}(\mathbf{h}) = \frac{1}{[(2\pi)^{2N} \det \boldsymbol{\Sigma}]^{1/2}} \exp \left[-\frac{1}{2}(\mathbf{h} - \boldsymbol{\mu})^T \boldsymbol{\Sigma}^{-1}(\mathbf{h} - \boldsymbol{\mu}) \right]. \quad (11)$$

Here, $\boldsymbol{\mu} = (u_1, v_1, \dots, u_N, v_N)^T$ is the mean vector and $\boldsymbol{\Sigma} = \text{diag}(\sigma_1^2, \tau_1^2, \dots, \sigma_N^2, \tau_N^2)$ is the covariance matrix. Now, it can be verified that

$$\eta_{2j-1} = \mathbf{h}^T \mathbf{K}_1 \mathbf{t}_j, \quad \eta_{2j} = \mathbf{h}^T \mathbf{K}_2 \mathbf{t}_j, \quad (12)$$

for $j = 1, \dots, N$, where we have defined

$$\mathbf{K}_1 = \mathbf{1}_N \otimes \sigma_z, \quad \mathbf{K}_2 = \mathbf{1}_N \otimes \sigma_x, \quad (13)$$

with $\sigma_z = \begin{pmatrix} 1 & 0 \\ 0 & -1 \end{pmatrix}$ and $\sigma_x = \begin{pmatrix} 0 & 1 \\ 1 & 0 \end{pmatrix}$ being two of the Pauli matrices. Also, $\mathbf{t}_j = (C_{j,1}, S_{j,1}, \dots, C_{j,N}, S_{j,N})^T$. The joint probability density of the real and imaginary parts of eigenvalues of matrix \mathbf{H} can now be obtained by integrating over \mathbf{h} , viz.,

$$P(\boldsymbol{\eta}) = \int d\mathbf{h} P_{\mathbf{h}}(\mathbf{h}) \prod_{j=1}^N \delta(\eta_{2j-1} - \mathbf{h}^T \mathbf{K}_1 \mathbf{t}_j) \delta(\eta_{2j} - \mathbf{h}^T \mathbf{K}_2 \mathbf{t}_j). \quad (14)$$

It is convenient to perform the \mathbf{h} -integral by going to the Fourier space, $\{\eta_j \mapsto \zeta_j\}$. The resulting characteristics function is given by,

$$\begin{aligned} \Phi(\boldsymbol{\zeta}) &= \int \prod_{j=1}^{2N} d\eta_j \exp(i\zeta_j \eta_j) P(\boldsymbol{\eta}) \\ &= \int d\mathbf{h} P_{\mathbf{h}}(\mathbf{h}) \exp \left[i\mathbf{h}^T \sum_{j=1}^N (\mathbf{K}_1 \mathbf{t}_j \zeta_{2j-1} + \mathbf{K}_2 \mathbf{t}_j \zeta_{2j}) \right], \end{aligned} \quad (15)$$

where we used Eq. (12) to replace η_j . Now, we note that $\sum_{j=1}^N (\mathbf{K}_1 \mathbf{t}_j \zeta_{2j-1} + \mathbf{K}_2 \mathbf{t}_j \zeta_{2j}) = \mathbf{Q}\boldsymbol{\zeta}$, where

$$\mathbf{Q} = (\mathbf{K}_1 \mathbf{t}_1, \mathbf{K}_2 \mathbf{t}_1, \mathbf{K}_1 \mathbf{t}_2, \mathbf{K}_2 \mathbf{t}_2, \dots, \mathbf{K}_1 \mathbf{t}_N, \mathbf{K}_2 \mathbf{t}_N),$$

is a $2N \times 2N$ -dimensional matrix and $\boldsymbol{\zeta} = (\zeta_1, \zeta_2, \dots, \zeta_{2N-1}, \zeta_{2N})^T$ is a $2N$ -dimensional column vector. Therefore, the above equation can be rewritten as,

$$\begin{aligned} \Phi(\boldsymbol{\zeta}) &= \int d\mathbf{h} P_{\mathbf{h}}(\mathbf{h}) \exp(i\mathbf{h}^T \mathbf{Q}\boldsymbol{\zeta}) \\ &= \int d\mathbf{h} \frac{1}{[(2\pi)^{2N} \det \boldsymbol{\Sigma}]^{1/2}} \exp \left[-\frac{1}{2}(\mathbf{h} - \boldsymbol{\mu})^T \boldsymbol{\Sigma}^{-1}(\mathbf{h} - \boldsymbol{\mu}) + i\mathbf{h}^T \mathbf{Q}\boldsymbol{\zeta} \right]. \end{aligned} \quad (16)$$

The above multidimensional-Gaussian integral can be readily performed to yield

$$\Phi(\boldsymbol{\zeta}) = \exp \left(-\frac{1}{2} \boldsymbol{\zeta}^T \mathbf{T} \boldsymbol{\zeta} + i\boldsymbol{\nu}^T \boldsymbol{\zeta} \right), \quad (17)$$

where $\boldsymbol{\nu} = \mathbf{Q}^T \boldsymbol{\mu}$ and $\mathbf{T} = \mathbf{Q}^T \boldsymbol{\Sigma} \mathbf{Q}$. We now perform the inverse Fourier transform and return back to the η space, leading us to the desired expression,

$$P(\boldsymbol{\eta}) = \frac{1}{[(2\pi)^{2N} \det \mathbf{T}]^{1/2}} \exp \left[-\frac{1}{2}(\boldsymbol{\eta} - \boldsymbol{\nu})^T \mathbf{T}^{-1}(\boldsymbol{\eta} - \boldsymbol{\nu}) \right]. \quad (18)$$

This equation gives the joint probability density function of real and imaginary parts of the *ordered* eigenvalues of \mathbf{H} , as in Eq. (6). Evidently, it is a multivariate Gaussian distribution. An immediate consequence of this is that any marginals of the above is again a (multivariate)-Gaussian distribution. For instance, the joint distribution of $\eta_{j_1}, \dots, \eta_{j_r}$, with $r \leq 2N$ is given by

$$\tilde{P}(\tilde{\boldsymbol{\eta}}) = \frac{1}{[(2\pi)^r \det \tilde{\mathbf{T}}]^{1/2}} \exp \left[-\frac{1}{2}(\tilde{\boldsymbol{\eta}} - \tilde{\boldsymbol{\nu}})^T \tilde{\mathbf{T}}^{-1}(\tilde{\boldsymbol{\eta}} - \tilde{\boldsymbol{\nu}}) \right], \quad (19)$$

where the quantities with tilde on top have been obtained by removing all variables/parameters having indices other than j_1 to j_r in Eq. (18). In particular, the marginal density involving the real (η_{2j-1}) and imaginary (η_{2j}) parts of a specific λ_j is given by Eq. (19) with $\tilde{\boldsymbol{\eta}} = \begin{pmatrix} \eta_{2j-1} \\ \eta_{2j} \end{pmatrix}$, $\tilde{\boldsymbol{\nu}} = \begin{pmatrix} \nu_{2j-1} \\ \nu_{2j} \end{pmatrix}$, $\tilde{\mathbf{T}} = \begin{pmatrix} T_{2j-1,2j-1} & T_{2j-1,2j} \\ T_{2j,2j-1} & T_{2j,2j} \end{pmatrix}$. Notably, the marginal density of a single component η_j is just a Gaussian distribution,

$$p(\eta_j) = \frac{1}{(2\pi T_{jj})^{1/2}} \exp \left[-\frac{(\eta_j - \nu_j)^2}{2T_{jj}} \right]. \quad (20)$$

The above expressions give the distribution of the eigenvalue(s) ordered according to the ordering of the N th roots of unity, as in Eq. (6). The joint distribution of unordered η_j can be obtained by symmetrizing Eq. (18) in all eigenvalues. Therefore, the joint

probability density of real and imaginary parts of *unordered* eigenvalues of \mathbf{H} is given by

$$\widehat{P}(\boldsymbol{\eta}) = \frac{1}{N!} \sum_{\{j\}} \frac{1}{[(2\pi)^{2N} \det \mathcal{T}^{\{j\}}]^{1/2}} \exp \left[-\frac{1}{2} (\boldsymbol{\eta} - \boldsymbol{\nu}^{\{j\}})^T (\mathcal{T}^{\{j\}})^{-1} (\boldsymbol{\eta} - \boldsymbol{\nu}^{\{j\}}) \right], \quad (21)$$

where

$$\boldsymbol{\nu}^{\{j\}} = (\nu_{j_1}, \nu_{j_2}, \dots, \nu_{j_{2N-1}}, \nu_{j_{2N}})^T,$$

$$\mathcal{T}^{\{j\}} = \begin{pmatrix} T_{j_1, j_1} & T_{j_1, j_2} & \cdots & T_{j_1, j_{2N-1}} & T_{j_1, j_{2N}} \\ T_{j_2, j_1} & T_{j_2, j_2} & \cdots & T_{j_2, j_{2N-1}} & T_{j_2, j_{2N}} \\ \vdots & \vdots & \ddots & \vdots & \vdots \\ T_{j_{2N-1}, j_1} & T_{j_{2N-1}, j_2} & \cdots & T_{j_{2N-1}, j_{2N-1}} & T_{j_{2N-1}, j_{2N}} \\ T_{j_{2N}, j_1} & T_{j_{2N}, j_2} & \cdots & T_{j_{2N}, j_{2N-1}} & T_{j_{2N}, j_{2N}} \end{pmatrix},$$

such that the sum in Eq. (21) involves the $N!$ permutations of index-pairs $\{(j_1, j_2), (j_3, j_4), \dots, (j_{2N-1}, j_{2N})\}$ over the pairs $\{(1, 2), (3, 4), \dots, (2N-1, 2N)\}$. From this, the marginal distributions can be obtained by integrating out the unwanted η -variables. For example, the unordered counterpart of Eq. (20), i.e., probability density of real part or the imaginary part of a generic eigenvalue of \mathbf{H} will be a sum of Gaussians, i.e.,

$$\widehat{p}_{\text{Re}}(\eta) = \frac{1}{N} \sum_{j=1}^N \frac{1}{(2\pi T_{2j-1, 2j-1})^{1/2}} \exp \left[-\frac{(\eta - \nu_{2j-1})^2}{2T_{2j-1, 2j-1}} \right], \quad (22)$$

$$\widehat{p}_{\text{Im}}(\eta) = \frac{1}{N} \sum_{j=1}^N \frac{1}{(2\pi T_{2j, 2j})^{1/2}} \exp \left[-\frac{(\eta - \nu_{2j})^2}{2T_{2j, 2j}} \right]. \quad (23)$$

3 Explicit evaluations of \mathbf{T} and $\boldsymbol{\nu}$

In this section, we provide explicit expressions for covariance matrix \mathbf{T} and mean vector $\boldsymbol{\nu}$ of Eq. (18) in terms of the averages and variances of matrix elements of \mathbf{A} and \mathbf{B} . From the definition of $\mathbf{T} = \mathbf{Q}^T \boldsymbol{\Sigma} \mathbf{Q}$, and noting from Eq. (13) that $\mathbf{K}_1^T = \mathbf{K}_1$, $\mathbf{K}_2^T = \mathbf{K}_2$, it follows that the matrix elements of \mathbf{T} are given by

$$T_{2l-1, 2m-1} = \mathbf{t}_l^T \mathbf{K}_1 \boldsymbol{\Sigma} \mathbf{K}_1 \mathbf{t}_m = \sum_{r=1}^N (\sigma_r^2 C_{l,r} C_{m,r} + \tau_r^2 S_{l,r} S_{m,r}), \quad (24)$$

$$T_{2l-1, 2m} = \mathbf{t}_l^T \mathbf{K}_1 \boldsymbol{\Sigma} \mathbf{K}_2 \mathbf{t}_m = \sum_{r=1}^N (\sigma_r^2 C_{l,r} S_{m,r} - \tau_r^2 S_{l,r} C_{m,r}), \quad (25)$$

$$T_{2l,2m-1} = \mathbf{t}_l^T \mathbf{K}_2 \Sigma \mathbf{K}_1 \mathbf{t}_m = \sum_{r=1}^N (\sigma_r^2 S_{l,r} C_{m,r} - \tau_r^2 C_{l,r} S_{m,r}), \quad (26)$$

$$T_{2l,2m} = \mathbf{t}_l^T \mathbf{K}_2 \Sigma \mathbf{K}_2 \mathbf{t}_m = \sum_{r=1}^N (\sigma_r^2 S_{l,r} S_{m,r} + \tau_r^2 C_{l,r} C_{m,r}), \quad (27)$$

for $l, m = 1, 2, \dots, N$. Similarly, for the mean vector $\boldsymbol{\nu}$, we obtain

$$\nu_{2l-1} = \mathbf{t}_j^T \mathbf{K}_1 \boldsymbol{\mu} = \sum_{r=1}^N [C_{l,r} u_r - S_{l,r} v_r], \quad (28)$$

$$\nu_{2l} = \mathbf{t}_j^T \mathbf{K}_2 \boldsymbol{\mu} = \sum_{r=1}^N [C_{l,r} v_r + S_{l,r} u_r], \quad (29)$$

for $l = 1, \dots, N$. Some special cases of the above deserve further discussion, as outlined below.

3.0.1 Some special cases of the covariance matrix \mathbf{T}

- $\sigma_r = \tau_r$ for $r = 1, \dots, N$

In this case

$$T_{2l-1,2m-1} = \sum_{r=1}^N \sigma_r^2 \cos \left[\frac{2\pi(l-m)(N-r+1)}{N} \right], \quad (30)$$

$$T_{2l-1,2m} = - \sum_{r=1}^N \sigma_r^2 \sin \left[\frac{2\pi(l-m)(N-r+1)}{N} \right], \quad (31)$$

$$T_{2l,2m-1} = \sum_{r=1}^N \sigma_r^2 \sin \left[\frac{2\pi(l-m)(N-r+1)}{N} \right], \quad (32)$$

$$T_{2l,2m} = \sum_{r=1}^N \sigma_r^2 \cos \left[\frac{2\pi(l-m)(N-r+1)}{N} \right], \quad (33)$$

for $l, m = 1, 2, \dots, N$.

- $\sigma_r = \tau_r = \sigma$ for $r = 1, \dots, N$

In this case, we obtain

$$\begin{aligned} T_{2l-1,2m-1} &= T_{2l,2m} \\ &= \sigma^2 \sum_{r=1}^N \cos \left[\frac{2\pi(l-m)(N-r+1)}{N} \right] \\ &= \sigma^2 \sum_{r=1}^N \delta_{l,m} = N\sigma^2 \delta_{l,m}, \end{aligned} \quad (34)$$

where $\delta_{l,m}$ is the the Kronecker delta. On the other hand,

$$\begin{aligned} T_{2l-1,2m} &= -T_{2l,2m-1} \\ &= -\sigma^2 \sum_{r=1}^N \sin \left[\frac{2\pi(l-m)(N-r+1)}{N} \right] \\ &= 0. \end{aligned} \tag{35}$$

Therefore, overall, in this case we have

$$\mathbf{T} = N\sigma^2 \mathbf{1}_{2N}, \tag{36}$$

which means that the η 's become independent Gaussians.

- $\tau_r \rightarrow 0$ for $r = 1, \dots, N$

In this case, the elements $T_{2l,2l}$ warrant special attention. From Eq. (27), we find that they simplify to $\sum_{r=1}^N \sigma_r^2 S_{l,r}^2$. Now, $S_{l,r} = \sin[2\pi(l-1)(N-r+1)/N]$, which vanishes for all $r = 1, \dots, N$ if $2(l-1)/N$ is an integer. This happens for $l = 1$ and additionally when $l = N/2 + 1$ if N is even.

Working in a limiting sense, the consequence of this is that the variance $T_{2,2}$ tends to zero in the Gaussian density (18) for η_2 and gives a Dirac delta function $\delta(\eta_2 - \nu_2)$, thereby effectively making the imaginary part of the eigenvalue λ_1 of \mathbf{H} to assume a fixed value of ν_2 for both even and odd N , i.e., $\Im(\lambda_1) \rightarrow \nu_2$. Additionally, in the even N case, $\Im(\lambda_{N/2+1}) \rightarrow \nu_{N+2}$. If on top of this, the corresponding averages ν (see below) are zero, then these eigenvalues become purely real. Therefore, a real circulant matrix will necessarily possess one real eigenvalue when N is odd and two real eigenvalues when N is even. The remaining eigenvalues occur in complex-conjugate pairs.

- $\sigma_r \rightarrow 0$ for $r = 1, \dots, N$

This case is similar to the last one and now $T_{2l-1,2l-1}$ becomes 0 when $l = 1$ for both even and odd N , and additionally when $l = N/2 + 1$ for even N . Thus, here $\Re(\lambda_1)$ tends to a fixed value of ν_1 , i.e., $\Re(\lambda_1) \rightarrow \nu_1$. Moreover, when N is even, $\Re(\lambda_{N/2+1}) \rightarrow \nu_{N+1}$. Moreover, if the averages ν are zero, then these eigenvalues will be purely imaginary. The other eigenvalues occur in $\pm x + iy$ ($x, y \in \mathbb{R}$) pairs. This is in consonance with the preceding case, as now we have a purely imaginary circulant matrix.

3.0.2 Some special cases for the mean vector $\boldsymbol{\nu}$

- $u_r = v_r = u$ for $r = 1, \dots, N$

In this case, we find that

$$\boldsymbol{\nu}_{2l-1} = \boldsymbol{\nu}_{2l} = Nu\delta_{l,1}. \tag{37}$$

Consequently, we have

$$\boldsymbol{\nu} = (Nu, Nu, 0, \dots, 0)^T. \tag{38}$$

- $u_r = u$ and $v_r = 0$ for $r = 1, \dots, N$

In this case, we have

$$\boldsymbol{\nu}_{2l-1} = Nu\delta_{l,1}, \quad \boldsymbol{\nu}_{2l} = 0, \quad (39)$$

for $l = 1, \dots, N$.

- $u_r = 0$ and $v_r = v$ for $r = 1, \dots, N$

$$\boldsymbol{\nu}_{2l-1} = 0, \quad \boldsymbol{\nu}_{2l} = Nv\delta_{l,1}, \quad (40)$$

for $l = 1, \dots, N$.

4 Wigner-like matrix model based on \mathbf{H}

The Wigner matrix model $(\mathbf{G} + \mathbf{G}^\dagger)/2$, where \mathbf{G} is a square matrix with independent and identically distributed (iid) zero mean Gaussian elements (Ginibre random matrix), is arguably the most popular one in the theory of random matrices [25, 26]. It corresponds to the classic Gaussian ensembles, specifically Gaussian Orthogonal Ensemble (GOE) when \mathbf{G} is real and Gaussian Unitary Ensemble (GUE) when \mathbf{G} is complex. As one moves away from the iid, zero mean set-up, deviations from the classic case is observed. We examine below this matrix model with \mathbf{G} replaced by the circulant matrix \mathbf{H} and study its eigenvalues.

Employing the eigenvalue decomposition $\mathbf{H} = \mathbf{U}^\dagger \boldsymbol{\Lambda} \mathbf{U}$, it is easy to see that we have

$$\mathbf{R} := \frac{\mathbf{H} + \mathbf{H}^\dagger}{2} = \mathbf{U}^\dagger \frac{(\boldsymbol{\Lambda} + \boldsymbol{\Lambda}^\dagger)}{2} \mathbf{U} = \mathbf{U}^\dagger \Re(\boldsymbol{\Lambda}) \mathbf{U}, \quad (41)$$

which shows that the eigenvalues λ_l^R of \mathbf{R} are just the real part of eigenvalues of \mathbf{H} , i.e., $\lambda_l^R = \eta_{2l-1}$ for $l = 1, \dots, N$. In a similar manner, we have,

$$\mathbf{J} := \frac{\mathbf{H} - \mathbf{H}^\dagger}{2i} = \mathbf{U}^\dagger \frac{(\boldsymbol{\Lambda} - \boldsymbol{\Lambda}^\dagger)}{2i} \mathbf{U} = \mathbf{U}^\dagger \Im(\boldsymbol{\Lambda}) \mathbf{U}. \quad (42)$$

Therefore, the eigenvalues λ_l^J of \mathbf{J} are the imaginary part of the eigenvalues of \mathbf{H} , i.e., $\lambda_l^J = \eta_{2l}$ for $l = 1, \dots, N$. In both cases, the joint distribution of these eigenvalues, as well as their marginals follow from the results in Sec. I. These are completely different from the classical case, where the exact eigenvalue distributions are expressible in terms of weighted Hermite polynomials [25, 26].

5 Wishart-like matrix model based on \mathbf{H}

Another one of the classical random matrix model is the so called Wishart model, $\mathbf{G}\mathbf{G}^\dagger$, where \mathbf{G} is again a square Gaussian random matrix as above. In the general case, however, it can be rectangular also. For real \mathbf{G} one gets the Laguerre Orthogonal

Ensemble (LOE) and for complex \mathbf{G} one has Laguerre Unitary Ensemble (LUE). Here, we replace \mathbf{G} by the circulant matrix \mathbf{H} and try to see how the eigenvalue statistics deviate from the classical case. Thus, we have,

$$\mathbf{W} := \mathbf{H}\mathbf{H}^\dagger = (\mathbf{U}^\dagger \mathbf{\Lambda} \mathbf{U})(\mathbf{U}^\dagger \mathbf{\Lambda}^\dagger \mathbf{U}) = \mathbf{U}^\dagger |\mathbf{\Lambda}|^2 \mathbf{U}, \quad (43)$$

since $\mathbf{U}\mathbf{U}^\dagger = \mathbb{1}_N$. Therefore, the eigenvalues λ_l^W of \mathbf{W} are modulus-squared eigenvalues of \mathbf{H} , i.e., $\lambda_l^W = \eta_{2l-1}^2 + \eta_{2l}^2$ for $l = 1, \dots, N$. The joint probability density for these eigenvalues can be obtained using,

$$P(\lambda_1^W, \dots, \lambda_N^W) = \int d\boldsymbol{\eta} P(\boldsymbol{\eta}) \prod_{l=1}^N \delta(\lambda_l^W - \eta_{2l-1}^2 - \eta_{2l}^2). \quad (44)$$

Let us consider the corresponding multidimensional Laplace transform ($\{\lambda_l^W \mapsto s_l\}$),

$$\Psi(s_1, \dots, s_N) = \int d\boldsymbol{\eta} P(\boldsymbol{\eta}) \prod_{l=1}^N e^{-s_l(\eta_{2l-1}^2 + \eta_{2l}^2)}. \quad (45)$$

Defining $\mathbf{S} = \bigoplus_{l=1}^N (s_l \otimes \mathbb{1}_2) = \text{diag}(s_1, s_1, s_2, s_2, \dots, s_N, s_N)$, and inserting the expression of $P(\boldsymbol{\eta})$ from Eq. (18), we obtain,

$$\Psi(s_1, \dots, s_N) = \frac{1}{[(2\pi)^{2N} \det \mathbf{T}]^{1/2}} \int d\boldsymbol{\eta} \exp[-\boldsymbol{\eta}^T \mathbf{S} \boldsymbol{\eta}] \exp\left[-\frac{1}{2}(\boldsymbol{\eta} - \boldsymbol{\nu})^T \mathbf{T}^{-1}(\boldsymbol{\eta} - \boldsymbol{\nu})\right]. \quad (46)$$

This multidimensional Gaussian integral in η_i can be performed to yield

$$\Psi(s_1, \dots, s_N) = \frac{\exp\left[\frac{1}{2}\boldsymbol{\nu}^T \{(\mathbf{T} + 2\mathbf{T}\mathbf{S}\mathbf{T})^{-1} - \mathbf{T}^{-1}\}\boldsymbol{\nu}\right]}{[\det(\mathbb{1}_N + 2\mathbf{S}\mathbf{T})]^{1/2}}. \quad (47)$$

Unfortunately, it does not seem feasible to perform the inverse Laplace transform to obtain the joint distribution of the eigenvalues. However, if we just focus on one of the eigenvalues (say λ_j^W) along with the assumption that the mean vector $\boldsymbol{\mu}$, and hence $\boldsymbol{\nu}$, is zero, then proceeding similar to above, we obtain the following expression for Laplace transform associated with the joint probability density of the real (η_{2j-1}) and imaginary (η_{2j}) parts,

$$\psi(s) = \frac{1}{[\det(\mathbb{1}_2 + 2s\tilde{\mathbf{T}})]^{1/2}}, \quad (48)$$

where $\tilde{\mathbf{T}}$ is as defined below Eq. (19). Now, if

$$t_j^\pm = \frac{(T_{2j-1,2j-1} + T_{2j,2j}) \pm \sqrt{(T_{2j-1,2j-1} + T_{2j,2j})^2 - 4T_{2j-1,2j}T_{2j,2j-1}}}{2},$$

be the eigenvalues of $\tilde{\mathbf{T}}$, i.e., then the above can be written as

$$\psi(s) = \frac{1}{[(1 + 2st_j^+)(1 + 2st_j^-)]^{1/2}}. \quad (49)$$

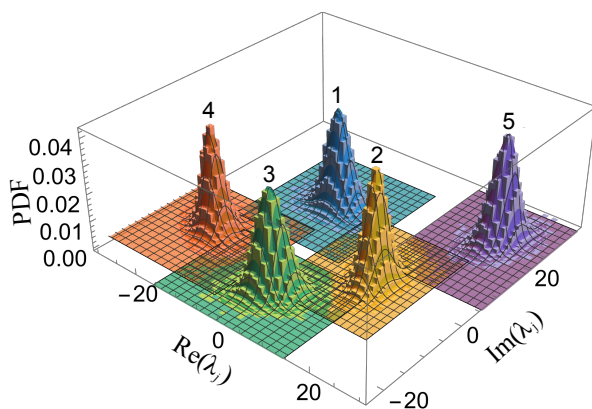


Figure 1. Probability densities of individual ordered eigenvalues of \mathbf{H} in the complex plane for $N = 5$. The averages and standard deviations of independent Gaussian elements of matrices \mathbf{A} and \mathbf{B} are $(u_1, u_2, u_3, u_4, u_5; \sigma_1, \sigma_2, \sigma_3, \sigma_4, \sigma_5) = (2, 9, -7, -19/2, -5/3; 1, 2, 1/2, 2/7, 4/5)$ and $(v_1, v_2, v_3, v_4, v_5; \tau_1, \tau_2, \tau_3, \tau_4, \tau_5) = (4, 8, -15/2, 3, 20/3; 6/5, 2/3, 3/4, 4/7, 3/5)$, respectively. The simulation results, obtained from an ensemble comprising 50000 matrices, are shown as histograms, while the two-dimensional surfaces are based on analytical result given in Eq. (19). The ordering of the eigenvalues has been indicated using the numbers above the histograms.

The inverse Laplace transform can then be performed to give [35],

$$p_W(\lambda_j^W) = \frac{1}{2(t_j^+ t_j^-)^{1/2}} \exp \left[- \left(\frac{1}{t_j^+} + \frac{1}{t_j^-} \right) \frac{\lambda_j^W}{4} \right] I_0 \left(\left| \frac{1}{t_j^+} - \frac{1}{t_j^-} \right| \frac{\lambda_j^W}{4} \right), \quad (50)$$

where $I_0(z)$ is the zeroth-order modified Bessel function of the first kind. If one examines the distribution of an eigenvalue without ordering, then the corresponding probability density function would be

$$\hat{p}_W(\lambda^W) = \frac{1}{N} \sum_{j=1}^N p_W(\lambda_j^W). \quad (51)$$

Compared to the classical Wishart ensemble, where the eigenvalue density is expressible in terms of weighted Laguerre polynomials, this result is again very different.

6 Comparison of analytical results with numerical simulations

In this section, we compare the analytical results obtained in the preceding sections with Monte Carlo numerical simulations of the relevant random matrix models. Firstly, we examine the eigenvalue density of ordered eigenvalues in the complex plane. Figure 1 presents an illustrative example based on an ensemble comprising 50000 \mathbf{H} matrices of size $N = 5$, displaying the probability density functions of individual eigenvalues using histograms in the complex plane. The figure caption provides the corresponding parameter values. The histograms, representing the numerical simulations, are compared to two-dimensional surfaces depicting the analytical results

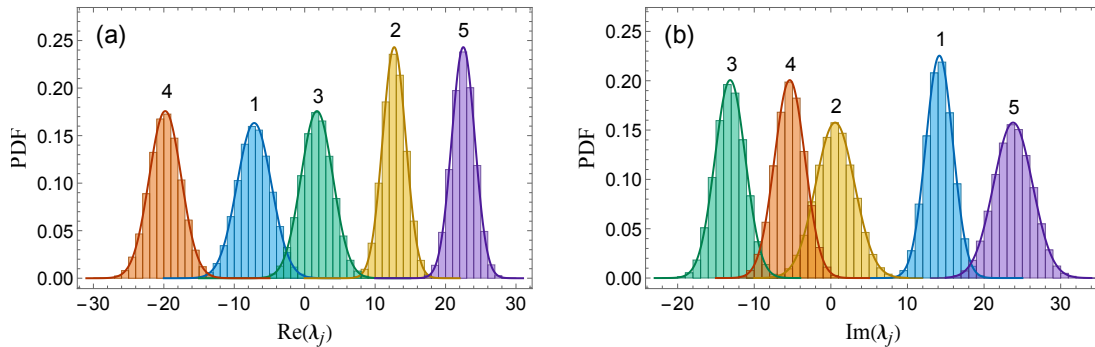


Figure 2. Probability densities of (a) real and (b) imaginary parts of individual ordered eigenvalues of \mathbf{H} . The parameter values are the same as those in figure 1. The histograms depict the results obtained from numerical simulations, while the solid lines represent the analytical results. The numbers above the histograms indicate the ordering of the eigenvalues.

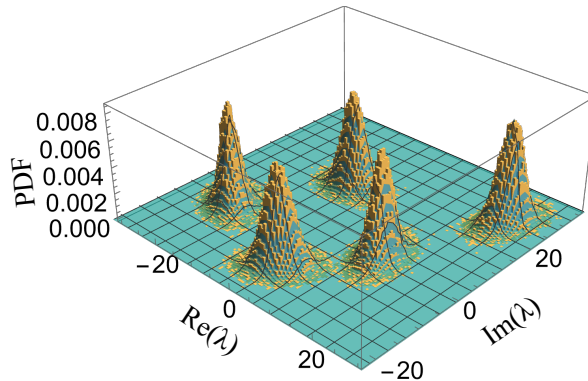


Figure 3. Probability density of an unordered eigenvalue of \mathbf{H} in the complex plane for $N = 5$. Parameter values and presentation scheme are as in figure 1. In this case, the analytical result employed is Eq. (21).

derived from Eq. (19). To further analyze the characteristics, we show the densities of the real and imaginary parts in figure 2. Again, histograms obtained from simulations are used, while solid lines represent the analytical expressions. For the same parameter values, figures 3 and 4 present results for the unordered eigenvalue case, utilizing Eqs. (21) to (23). We examine the impact of changing the means (v_j) and variances (τ_j^2) of matrix element in matrix \mathbf{B} on the eigenvalue density in figures 5 and 6 by employing 20000 \mathbf{H} matrices of dimension $N = 4$. By bringing these values close to zero in the second of these two figures (see captions), two eigenvalues approach the real line, while the other two tend to form complex conjugate pairs, as discussed in subsection 3.0.1. The first panel in both of these figures show the scatter plot of numerically generated eigenvalues in the complex plane along with density plot based on Eq. (21). These plots clearly demonstrates the expected behavior, reflecting excellent agreement with the analytical predictions. Additionally, the probability densities of the real and imaginary parts of the unordered eigenvalues are included in these figures.

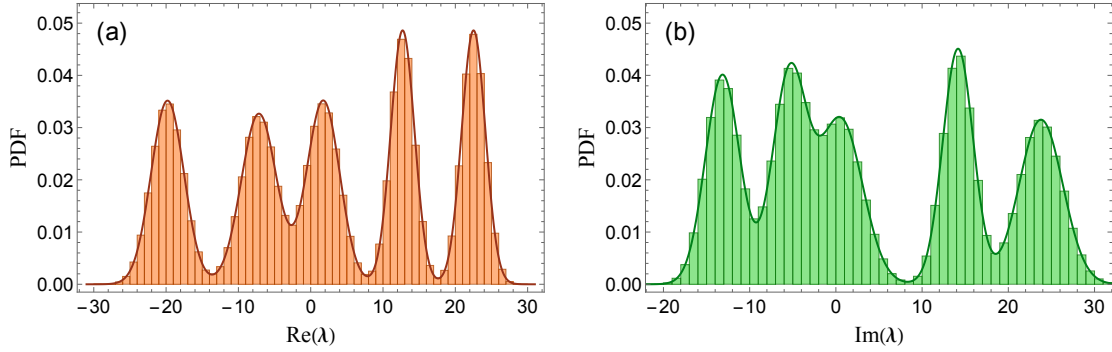


Figure 4. Probability densities of (a) real and (b) imaginary parts of an unordered eigenvalue of \mathbf{H} , corresponding to the one shown in figure 3. The histograms are obtained from numerical simulations, while the solid lines are derived from Eqs. (22) and (23).

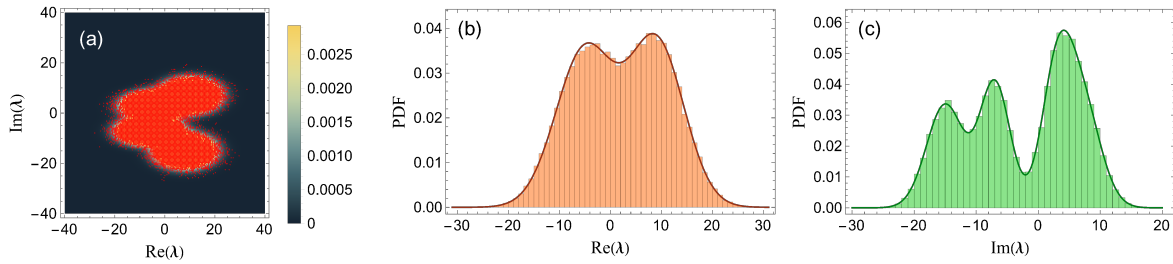


Figure 5. Distribution of an unordered eigenvalue of \mathbf{H} for $N = 4$. The averages and standard deviations of independent Gaussian elements of matrices \mathbf{A} and \mathbf{B} are $(u_1, u_2, u_3, u_4; \sigma_1, \sigma_2, \sigma_3, \sigma_4) = (2, 6, -7, -5; 5, 2, 1/2, 4/3)$ and $(v_1, v_2, v_3, v_4; \tau_1, \tau_2, \tau_3, \tau_4) = (-3, 2, 1, 3; 7/4, 3/2, 1/4, 5/6)$, respectively. Panel (a) shows the scatter plot of eigenvalues obtained from numerical simulation of 20000 matrices and the background density plot is using Eq. (21). Panels (b) and (c) illustrate the probability densities of the corresponding real and imaginary parts. The histograms are based on the numerical simulation results, while the solid lines represent the densities calculated using Eqs. (22) and (23).

Lastly, figure 7 showcases the distribution of a generic eigenvalue of the Wishart-like matrix \mathbf{W} for $N = 3$ case with an ensemble comprising 20000 matrices. The other parameter values are mentioned in the figure caption. Once again, a high degree of agreement is observed between the numerical simulation and the analytical result given by Eq. (51) in this case.

7 Summary and conclusion

In this work, we considered a versatile random matrix model defined by $\mathbf{H} = \mathbf{A} + i\mathbf{B}$, where \mathbf{A} and \mathbf{B} are real circulant matrices with independent but non-identical Gaussian entries. Through rigorous analysis, we established the exact joint probability density

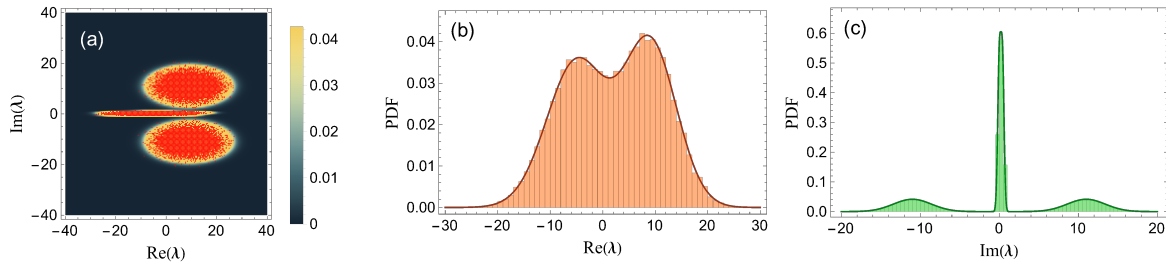


Figure 6. Plots as in figure 5 with all parameters same except those associated with matrix \mathbf{B} , given by $v_j = \tau_j = 1/10$, $j = 1, 2, 3, 4$, in this case. The impact of making the averages and variances of matrix \mathbf{B} close to zero is clearly seen. In consonance with the discussion in subsection 3.0.1, two eigenvalues approach the real line, while the other two tend to form complex conjugate pairs, leading to the results depicted above.

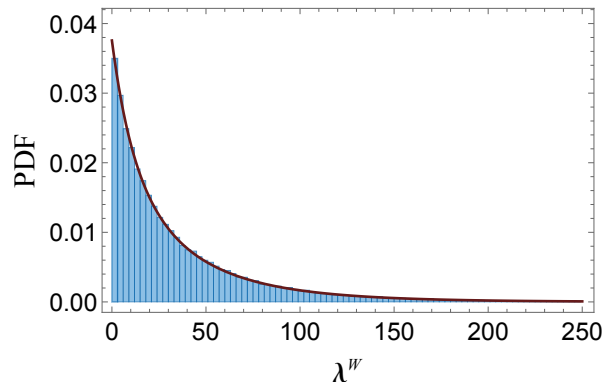


Figure 7. Probability density of an unordered eigenvalue of the matrix $\mathbf{W} = \mathbf{H}\mathbf{H}^\dagger$ for $N = 3$. The variances of independent zero-mean Gaussian elements of matrices \mathbf{A} and \mathbf{B} are $(\sigma_1, \sigma_2, \sigma_3) = (1, 7/2, 3/4)$ and $(\tau_1, \tau_2, \tau_3) = (4/3, 2/3, 9/2)$, respectively. The histogram has been obtained using numerical simulation comprising 20000 matrices and the solid line is based on Eq. (51).

function of this matrix model and demonstrated its multivariate Gaussian nature. This also enabled us to derive of marginal density functions of arbitrary order. By manipulating the averages and variances of the Gaussian elements, we showcased the model's ability to interpolate across a wide range of eigenvalue distributions in the complex plane, including those associated with the transition from random real circulant to complex circulant matrix. Additionally, we extended our investigation to include Wigner-like and Wishart-like matrices constructed from these random circulant matrices.

Prospective research could delve into numerous captivating directions. To illustrate, an avenue worthy of exploration involves the examination of circulant matrices-based variants of the elliptic Ginibre ensemble [27, 36, 37] and non-Hermitian Wishart matrices [38, 39] that are encompassed by the traditional Gaussian random matrices.

Moreover, exploring the implications of incorporating additional matrix structures or constraints within the present framework could lead to new insights. Additionally, investigating non-Gaussian distributions for the matrix entries and studying their impact on the eigenvalue distributions would provide valuable insights into the robustness of the model. Lastly, demonstrating explicit applications of the derived results in the areas mentioned in the introduction would be of notable interest.

Acknowledgments

S.S. and H.S. would like to thank Shiv Nadar Institution of Eminence for financial support. S.K. acknowledges the support provided by SERB, DST, Government of India, via Grant No. CRG/2022/001751.

References

- [1] Davis P J 1979 *Circulant Matrices* (New York: John Wiley & Sons), pp. 72–73
- [2] Gray R M 2006 *Toeplitz and Circulant Matrices: A Review* (The Netherlands: Now Publishers), pp. 21–22
- [3] Buzbee B L, Golub G H and Nielson C W 1970 On direct methods for solving Poisson’s equations *SIAM Journal on Numerical analysis* **7** 627
- [4] Wilde A C 1983 Differential equations involving circulant matrices *Rocky Mountain J Math.* **13** 1
- [5] Gilmour A E 1988 Circulant matrix methods for the numerical solution of partial differential equations by FFT convolutions *Appl. Math. Modelling* **12** 44
- [6] Delgado J, Romero N, Rovella A and Vilamajó F 2005 Bounded solutions of quadratic circulant difference equations *J. Difference Equ. Appl.* **11** 897
- [7] Chen W, Lin J and Chen CS 2013 The method of fundamental solutions for solving exterior axisymmetric Helmholtz problems with high wavenumber *Adv. Appl. Math Mech.* **5** 477
- [8] Elspas B and Turner J 1970 Graphs with circulant adjacency matrices *J. Comb. Theory* **9** 297
- [9] Vilfred V 2004 On circulant graphs, in Balakrishnan R, Sethuraman G, Wilson R J (eds.), *Graph Theory and its Applications* (Anna University, Chennai, March 14–16, 2001), Alpha Science, pp. 34–36.
- [10] Pollock D S G. 2002 Circulant matrices and time-series analysis *Internat. J. Math. Ed. Sci. Tech.* **33** 213
- [11] Fan J and Yao Q 2003 *Nonlinear Time Series* Springer Series in Statistics (New York: Springer-Verlag)
- [12] Brockwell P J and Davis R A 2006 *Time Series: Theory and Methods.* Springer Series in Statistics (New York: Springer)
- [13] Andrecut M 2008 Applications of left circulant matrices in signal and image processing *Modern Physics Letters B* **22** 231
- [14] Biemond J, Lagendijk R L and Mersereau R M 1990 Iterative methods for image deblurring *in Proceedings of the IEEE, vol. 78, no. 5, pp. 856-883*
- [15] Wittsack H J, Wohlschläger A M, Ritzl E K, Kleiser R, Cohnen M, Seitz R J and Mödder U 2008 CT-perfusion imaging of the human brain: Advanced deconvolution analysis using circulant singular value decomposition *Comput. Med. Imaging Graph.* **32** 67
- [16] Tiwari S, Das S S and Bandyopadhyay K K 2015 Precoded generalized frequency division multiplexing system to combat inter-carrier interference: Performance analysis *IET Commun.* **9** 1829

- [17] Henriques J F, Caseiro R, Martins P and Batista J 2012 Exploiting the circulant structure of tracking-by-detection with kernels *Proc. 12th Eur. Conf. Comput. Vis.*, 2012, pp. 702–715
- [18] Dou J, Qin Q and Tu Z 2017 Circulant structures based moving object detection *29th Chinese Control And Decision Conference (CCDC), Chongqing, China, 2017*, pp. 3331-3335
- [19] Daemen J and Rijmen V 2002 The design of Rijndael: AES-the advanced encryption standard (Berlin: Springer-Verlag)
- [20] MacWilliams F J and Sloane N J A 1988 *The theory of error correcting codes* (New Jersey: North Holland Publishing)
- [21] Olson B J, Shaw S W, Shi C, Pierre C and Parker R G 2014 Circulant matrices and their application to vibration analysis *Appl. Mech. Rev.* **66** 040803
- [22] Berlin T H and Kac M 1952 The Spherical Model of a Ferromagnet *Phys. Rev.* **86** 821
- [23] Santhanam T and Tekumalla A 1976 Quantum mechanics in finite dimensions *Found. Phys.* **6** 583
- [24] Aldrovandi R 2001 *Special Matrices of Mathematical Physics: Stochastic, Circulant, and Bell Matrices* (New Jersey: World Scientific)
- [25] Mehta M L 2004 *Random Matrices* (New York: Academic)
- [26] Forrester P J 2010 *Log-Gases and Random Matrices* (Princeton, NJ: Princeton University Press)
- [27] Byun S S and Forrester P J 2023 Progress on the study of the Ginibre ensembles I: GinUE *arXiv:2211.16223*
- [28] Byun S S and Forrester P J 2023 Progress on the study of the Ginibre ensembles II: GinOE and GinSE *arXiv:2301.05022*
- [29] Jain S R and Srivastava S C L 2008 Random cyclic matrices *Phys. Rev. E* **78** 036213
- [30] Jain S R and Srivastava S C L 2018 Pseudo-Hermitian Random matrix theory *Fortschritte der Phys.* **61** 276
- [31] Ali Md S. and Srivastava S C L 2022 Patterned random matrices: deviations from universality *J. Phys. A: Math. Theor.* **55** 495201
- [32] Meckes M W 2009 Some results on random circulant matrices, in *High Dimensional Probability V: The Luminy Volume* IMS Collections, vol. 5, pp. 213-223 (Beachwood: Institute of Mathematical Statistics)
- [33] Bose A and Saha K 2018 *Random Circulant Matrices* (Florida: CRC Press)
- [34] Bose A 2018 *Patterned Random Matrices* (Florida: CRC Press)
- [35] Bateman H 1954 *Tables of Integral Transforms, Vol. 1*, p. 236 (McGraw-Hill, New York, 1954).
- [36] Akemann G, Duits M and Molag L D 2023 The elliptic Ginibre ensemble: A unifying approach to local and global statistics for higher dimensions *J. Math. Phys.* **64** 023503
- [37] Molag L D 2023 Edge behavior of higher complex-dimensional determinantal point processes, *Ann. Henri Poincaré*. <https://doi.org/10.1007/s00023-023-01333-x>
- [38] Akemann G, Byun S-S and Kang N G 2021 A non-Hermitian generalization of the Marchenko-pasture distribution: from the circular law to multi-criticality *Ann. Henri Poincaré* **22** 1035
- [39] Bhattacharjee M, Bose A, and Dey A 2023 Joint convergence of sample cross-covariance matrices, *ALEA Lat. Am. J. Probab. Math. Stat.* **20** 395